SOILS AND FOUNDATIONS Vol. 50, No. 4, 471–482, Aug. 2010
Japanese Geotechnical Society

NUMERICAL ANALYSIS OF THE EROSION AND THE TRANSPORT OF FINE PARTICLES WITHIN SOILS LEADING TO THE PIPING PHENOMENON

KAZUNORI FUJISAWA[i], AKIRA MURAKAMI[ii] and SHIN-ICHI NISHIMURA[iii]

ABSTRACT

About 50% of the world's dam failures are triggered by piping, which is a primary cause of embankment breaks. The phenomenon of piping results from the erosion of soil particles and their transport within a soil mass. In this paper, a numerical method is proposed to analyze the erosion within soils and the transport of eroded soil particles by adopting the concept of the erosion rate of soils. In such an analysis, the saturated-unsaturated seepage flow of the pore liquid, the detachment of the soil particles from the soil fabric, and the migration of the eroded particles are taken into consideration, and the equations related to the conservation of the pore liquid and the eroded soil particles are numerically solved. This numerical simulation allows for the procurement of the temporal alteration and the spatial distribution of the porosity, the particle size distribution, and the concentration of the detached soil particles in the pore liquid, as well as the distribution of pore liquid pressure. The results have revealed that the method can reproduce the experimental data from previous studies on the internal erosion of soils and that it qualitatively predicts, from the numerical experiments, the typical development of piping within soils, such as soil blocks and embankments, as the solutions to the initial and the boundary value problems of the governing equations.

Key words: erosion, numerical analysis, seepage (**IGC**: A10/E7/E13)

INTRODUCTION

Piping is a phenomenon whereby a flow path, where the seepage flow is concentrated, appears within soil structures. This flow path is usually created due to the erosion and the migration of soil particles inside of structures. Piping is widely regarded as the primary cause of dam breaks. Actually, Foster et al. (2000a, b) investigated world-wide embankment dam failures and accidents, and reported that 46% of them were triggered by piping. Water leakage from aging irrigation ponds, which are small embankment dams used to store irrigation water, has frequently been reported in Japan. This leakage is attributed to piping in most cases. Since piping presents such a serious problem for soil structures subjected to seepage flow, the need to predict and prevent it is apparent.

The numerous studies done on piping can be roughly divided into two categories: boiling studies and internal erosion studies. Boiling is the failure of a soil skeleton induced by an intergranular seepage force greater than the resistible force of the soil mass due to its weight. The studies on boiling have been focused on the determination of the critical hydraulic head or the gradient (e.g., Meyer et al., 1994; Ojha et al., 2003). Internal erosion is the detachment of fine particles from the soil fabric due to the seepage flow and the transport of these particles out of the soil mass, which increases porosity and leads to piping (e.g., Khilar et al., 1985; Reddi et al., 2000; Wan and Fell, 2004). Unlike boiling, internal erosion does not cause the failure of the soil fabric, but these two phenomena are related to each other, as was shown by Skempton and Brogan (1994). They carried out boiling experiments, using mixtures of gravels and sands, and observed that the critical hydraulic gradient became even smaller than the conventional estimate when the sands in the mixture started to move and were transported by the seepage flow through the sample. Their results showed that internal erosion leads to the instability of the soil, and remains important even when boiling is the focus of attention.

Richards and Reddy (2007) pointed out the limitations in the current computational methods for evaluating the piping potential. Though piping is closely related to internal erosion, dealing with the internal erosion of soils and the transport of eroded soil particles in the field of soil mechanics is difficult using existing methods because the movement and the migration of the particles is not considered. The objective of this study is to propose a numerical method for analyzing the piping potential in terms of erosion and to verify the applicability and the capability of the method. To make it possible to work with the ero-

[i] Assistant Professor, Graduate School of Environmental Science, Okayama University, Japan (kazunori@cc.okayama-u.ac.jp).
[ii] Professor, Graduate School of Agriculture, Kyoto University, Japan.
[iii] Associate Professor, Graduate School of Environmental Science, Okayama University, Japan.
The manuscript for this paper was received for review on August 14, 2009; approved on April 5, 2010.
Written discussions on this paper should be submitted before March 1, 2011 to the Japanese Geotechnical Society, 4-38-2, Sengoku, Bunkyo-ku, Tokyo 112-0011, Japan. Upon request the closing date may be extended one month.

sion of soils, the concept of an erosion rate was employed. The erosion rate of soils is defined as the volume (or the mass) of the eroded particles per unit surface area within a unit of time, and it has been investigated and used in various fields of study (e.g., Ariathurai and Arulanandan, 1978; Robinson and Hanson, 1994; Izumi and Parker, 2000). It has been empirically shown that the erosion rate is given as a function of the applied shear stress on the surface of soil particles, although the theoretical interpretation is still under discussion (e.g., Shaikh et al., 1988; Briaud et al., 2001; Indraratna et al., 2009).

To be able to work with internal erosion and the transport of eroded fine particles within soils, the following must be considered: (1) the velocity field of the intergranular saturated-unsaturated seepage flow, (2) the increase in the porosity of soils owing to the erosion, and (3) the transportation of the eroded soil particles through the soil pores. In this paper, the governing equations for the above three items are introduced with Eulerian formulation, and a numerical method to solve the equations is proposed using the finite element method and a finite volume approach. The proposed numerical model is applied to experimental results and its feasibility is ascertained. In addition, numerical simulations of the piping development within a soil block and an embankment are carried out in order to demonstrate the capability of the method.

GOVERNING EQUATIONS

Erosion Rate and the Four Phases of Soils

Before deriving the governing equations, in this section we will introduce the erosion rate of soils and the soil phases. The erosion rate is defined as the volume of the eroded soil particles from the unit surface area of the erodible region within a unit of time, with a velocity dimension. Earlier empirical studies and recent semi-theoretical investigations adopted the following form for the erosion rate as a function of the shear stress exerted onto the erodible soil particles (e.g., Khilar et al., 1985; Reddi et al., 2000; Indraratna et al., 2009):

$$E=\alpha(\tau-\tau_c) \tag{1}$$

where E, α, τ, and τ_c denote the erosion rate, the erodibility coefficient, the shear stress, and the critical shear stress, respectively. If shear stress τ, exerted by a fluid, is smaller than critical shear stress τ_c, erosion does not occur.

Figure 1 shows the four phases of soils which need to be understood before internal erosion and the transport of the detached soil particles from the soil skeleton can be fully grasped. Soils are usually divided into three phases, namely, pore air, pore water, and soil particles. When considering the internal erosion of soils, however, there are essentially only two types of soil particles, i.e., the particles of the soil skeleton and those eroded or detached from the soil fabric.

As shown in Fig. 1, the mixture of pore water and eroded soil particles is defined as the pore liquid in this

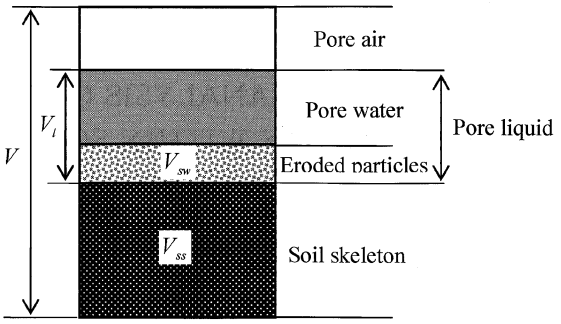

Fig. 1. Four phases of soils for considering internal erosion

paper. V, V_{ss}, V_{sw}, and V_l denote the volume of the soil mass, the soil skeleton, the eroded soil particles, and the pore liquid, respectively. Using these definitions, the soil properties are introduced as follows:

$$\theta=\frac{V_l}{V},\quad n=1-\frac{V_{ss}}{V},\quad C=\frac{V_{sw}}{V_l} \tag{2}$$

where θ, n, and C denote the volumetric liquid content, the porosity, and the concentration of detached soil particles from the soil fabric contained in the pore water, respectively.

Derivation of the Governing Equations

A two-dimensional problem is treated in this study. Fujisawa et al. (2009) have proposed the equations and the numerical method to analyze the loss of soil particles in saturated soils. Their method is developed in this section to consider both the seepage and the erosion in the saturated and unsaturated region. Figure 2 shows the volumetric balance of the pore liquid within an infinitesimal element, Δx_1 in width and Δx_2 in height. x_1, x_2, v_1, v_2, and A_e in the figure denote the horizontal and the vertical axes, the horizontal and the vertical components of the pore liquid velocity, and the surface area of the erodible region per unit volume, respectively.

Considering the direction of x_1, the pore liquid flows into the small soil element at a rate of $v_1\Delta x_2$ and flows out of it at a rate of $v_1\Delta x_2+\partial v_1/\partial x_1\Delta x_1\Delta x_2$, so that the pore liquid within the element decreases by $\partial v_1/\partial x_1\Delta x_1\Delta x_2$ due to the flow in the horizontal direction. Similarly, the pore liquid decreases by $\partial v_2/\partial x_2\Delta x_1\Delta x_2$ due to the flow in the vertical direction. In addition to the inflow and the outflow, the pore liquid increases according to the volume of the eroded soil particles, since the pore liquid is a mixture of pore water and eroded particles. The volume of the eroded soil particles per a unit of time is given by $EA_e\Delta x_1\Delta x_2$. From the above discussion, the rate of change in volumetric liquid content $\partial\theta/\partial t$ has the following relation:

$$\frac{\partial\theta}{\partial t}\Delta x_1\Delta x_2=(EA_e)\Delta x_1\Delta x_2-\frac{\partial v_1}{\partial x_1}\Delta x_1\Delta x_2-\frac{\partial v_2}{\partial x_2}\Delta x_1\Delta x_2 \tag{3}$$

The internal erosion decreases the volume of the soil skeleton by that of the eroded particles, which leads to the following equation:

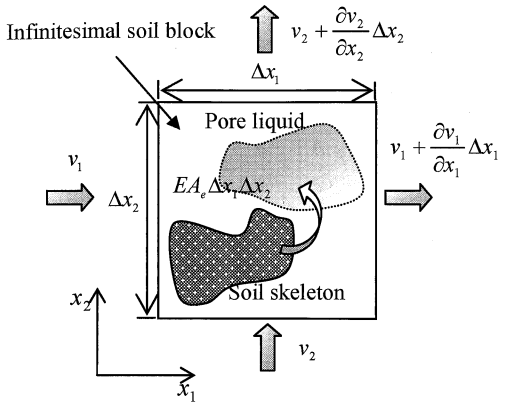

Fig. 2. Balance of pore liquid within infinitesimal soil block

$$\frac{\partial(1-n)}{\partial t}\Delta x_1\Delta x_2 = -EA_e\Delta x_1\Delta x_2 \tag{4}$$

The volume of eroded soil particles within the pore liquid also changes because of the inflow, the outflow, and the detachment of the soil particles from the fabric, which can be treated in the same manner as when deriving Eq. (3). Due to the horizontal and the vertical flows of pore liquid, the volume of the detached particles within the small element decreases by $\partial Cv_1/\partial x_1\Delta x_1\Delta x_2$ and $\partial Cv_2/\partial x_2\Delta x_1\Delta x_2$. Additionally, the soil particles are detached at a rate of $EA_e\Delta x_1\Delta x_2$. Therefore, the increase rate for the eroded soil particles within the small soil mass, $\partial C\theta/\partial t$, has the following relation:

$$\frac{\partial C\theta}{\partial t}\Delta x_1\Delta x_2 = (EA_e)\Delta x_1\Delta x_2 - \frac{\partial Cv_1}{\partial x_1}\Delta x_1\Delta x_2 - \frac{\partial Cv_2}{\partial x_2}\Delta x_1\Delta x_2 \tag{5}$$

Divided by $\Delta x_1\Delta x_2$, Eqs. (3) to (5) are reduced to the following three partial differential equations:

$$\frac{\partial\theta}{\partial t}+\frac{\partial v_i}{\partial x_i}=EA_e \tag{6}$$

$$\frac{\partial(1-n)}{\partial t}=-EA_e \tag{7}$$

$$\frac{\partial C\theta}{\partial t}+\frac{\partial Cv_i}{\partial x_i}=EA_e \tag{8}$$

where the Einstein summation convention is applied (the summation convention will be applied hereafter with respect to subscripts). A similar equation to Eq. (8) was adopted by Khilar et al. (1985) and Reddi and Bonala (1997) to analyze the migration of the eroded soil particles. The above three equations are adopted as the governing equations for the erosion within soils. The eroded soil particles can redeposited during their travel, but the redeposition process is ignored in this study since there is experimental evidence that redeposition can be ignored for small concentrations of soil particles in pore streams typical of natural subsurface systems (Gruesbeck and Collins, 1982; Reddi and Bonala, 1997). From an engineering viewpoint, it has been claimed that a consideration of redeposition may lead to an underestimation of soil erosion, which means that soil structures can be put at risk of deterioration.

Simplification of the Equations

Equation (7) is equivalent to

$$\frac{\partial n}{\partial t}=EA_e \tag{9}$$

With the aid of the relationship $\theta=nS_r$ and Eq. (9), Eq. (6) is rewritten as

$$n\frac{\partial S_r}{\partial t}+\frac{\partial v_i}{\partial x_i}=(1-S_r)EA_e \tag{10}$$

Internal erosion tends to be induced by a relatively rapid seepage flow. Therefore, assuming that erosion happens only in saturated zones, the right side of Eq. (10) vanishes because the degree of saturation S_r equals 1 when the soils are saturated and erosion rate E vanishes when the soils are unsaturated. This assumption and Darcy's law reduce Eq. (10) into the following form:

$$n\frac{\partial S_r}{\partial t}+\frac{\partial}{\partial x_i}\left(k\frac{\partial}{\partial x_i}\left(z+\frac{u_w}{\rho g}\right)\right)=0 \tag{11}$$

where k, h, z, u_w, ρ, and g denote the permeability, the hydraulic head, the elevation head, the pressure, the density of the pore liquid, and the gravitational acceleration, respectively. To solve Eq. (11), the van Genuchten model (van Genuchten, 1980) is used for the permeability and the water retention characteristics of soils as follows:

$$S_e=\frac{S_r-S_{rr}}{1-S_r}=\left[\frac{1}{1+(\alpha_G s)^{n_G}}\right]^{m_G},\quad s=u_w-u_a \tag{12}$$

$$k=k_S S_e^{1/2}\left[1-(1-S_e^{1/m_G})^{m_G}\right]^2 \tag{13}$$

where S_e, S_{rr}, s, u_a, and k_s denote the effective and the residual degree of saturation, suction, pore air pressure, and the saturated hydraulic conductivity, respectively, and pore air pressure u_a is usually constant. m_G and n_G in the above equations are the material constants which have the relationship $m_G=1-1/n_G$.

Estimation of Shear Stress

The shear stress exerted onto erodible soil particles needs to be estimated in order to evaluate the erosion rate of soils, as seen from Eq. (1). Efforts to estimate the shear stress in the interior of soils have required the idealization of the soil pores as an ensemble of pore tubes. Since the pore tube dimensions are distributed within the soils, determining the spatially distributed values of shear stress is challenge frequently overcome by using the representative pore tube dimensions. If the permeability and the porosity of a soil material are given, the representative pore diameter $\hat{D}$ is obtained as

$$\hat{D}=4\sqrt{2K/n} \tag{14}$$

where K denotes the intrinsic permeability, defined as

$$K=\frac{k_s\mu}{\rho g} \tag{15}$$

where μ is the viscosity of the pore liquid. Assuming the Hagen-Poiseulle flow in the pore tube, the shear stress exerted onto the pore wall is estimated by the following equation (e.g., Reddi et al., 2000):

$$\tau=\rho g I\sqrt{2K/n} \tag{16}$$

where I stands for the hydraulic gradient. The erosion rate can be determined with Eq. (16). The shear stress calculated by Eq. (16) is the averaged friction stress applied onto the pore wall. Since the surface area of the pore wall within a soil mass is usually large, the shear stress has small values under ordinary conditions. For example, when the hydraulic gradient is 1.0, the permeability of the soil mass is 1.0×10^{-5} m/s and the porosity is 0.5, the shear stress is calculated as 2.0×10^{-2} Pa, assuming a gravitational acceleration of 9.8 m/s^2, a water density of 1000 kg/m^3 and a viscosity of water of 1.0×10^{-3} Pa·s.

METHOD FOR THE NUMERICAL ANALYSIS

The numerical method for solving governing Eqs. (8), (9), and (11) is explained here. The unknown variables to be solved are the pressure of the pore liquid, u_w, porosity n, and the particle concentration within the pore liquid, C. Equation (11), which describes the seepage flow within soils, is solved with respect to the pressure of pore liquid u_w by the FEM (finite element method). In this analysis, a 4-node isoparametric element is adopted. FVM (finite volume method) is applied to solve Eq. (8) with respect to the concentration of eroded soil particles C. The utilization of FVM is especially easy when working with advection equations, such as Eq. (8), because the method does not require any inverse matrix calculations. Details of the application of FVM to Eq. (8) are given later in this section.

Figure 3 shows the flow chart for this computational analysis. Firstly, Eq. (11) is solved using the FEM (e.g., Neuman, 1973) and the results give the spatial distribution of the pressure for the pore liquid u_w. Supposing the calculation at the mth time step is completed, the hydraulic gradient I^m at the time step can be obtained from the calculated pressure of pore liquid u_w^m. In this paper, the numbers for the temporal and the spatial discretizations are consistently expressed as superscripts. From Darcy's law, the value of the seepage flow velocity is also available anywhere in the calculation region. Using Eq. (16), the determination of the hydraulic gradient allows for the evaluation of the shear stress. The erosion rate for material E^m can be estimated with the aid of Eq. (1). The surface area of the erodible region, which is equivalent to that of the movable soil particles, is evaluated either by a particle distribution curve or a test of the specific surface area. Given the erosion rate E^m and erodible surface area per unit volume A_e^m, the porosity increment is calculated from Eq. (9) as follows:

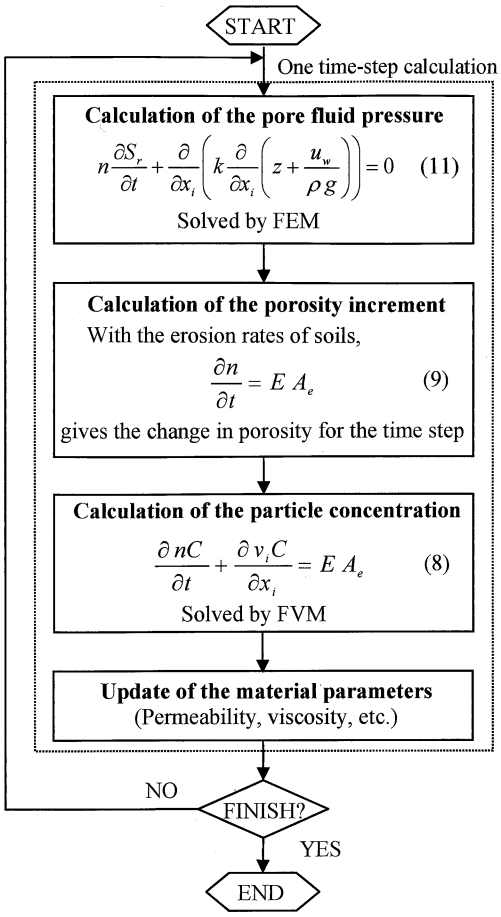

Fig. 3. Flow chart of the numerical analysis

$$n^{m+1}=n^m+\Delta t E^m A_e^m \tag{17}$$

where Δt is the time increment for one time step. (Note that the summation convention is not applied with respect to superscripts.) Equation (17) is calculated at the Gaussian integration points.

After the above process, Eq. (8), which describes the alteration of the particle concentration within the pore liquid, is solved with FVM. The finite elements of the above analysis are also used for the finite volume cells. FEM is applied to solve equations and to produce the typical values of variables at the nodal points, while FVM is used to compute the constant variables on the finite volume cells, which are the same as the finite volume elements in this study. Therefore, the values of variables, such as porosity n and seepage velocity v_i, are assigned for each cell with the Gaussian integral.

$$v_i^{l,m}=\frac{1}{V^l}\int_{\Omega^l} v_i^m dV^l \tag{18}$$

$$n^{l,m}=\frac{1}{V^l}\int_{\Omega^l} n^m dV^l \tag{19}$$

where Ω^l and V^l denote the region and the volume of the lth cell, respectively. $v_i^{l,m}$ and $n^{l,m}$ in Eqs. (18) and (19) are the representative values for the lth cell. By applying the FVM, Eq. (8) is spatially integrated in the cell.

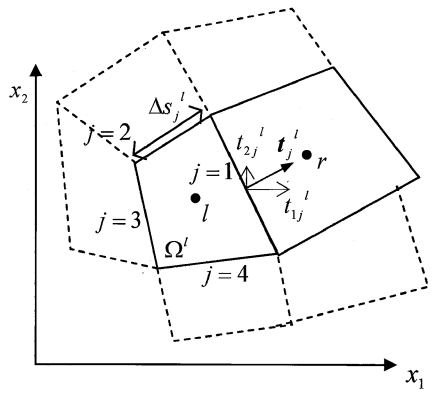

Fig. 4. Geometry of the finite volume cells

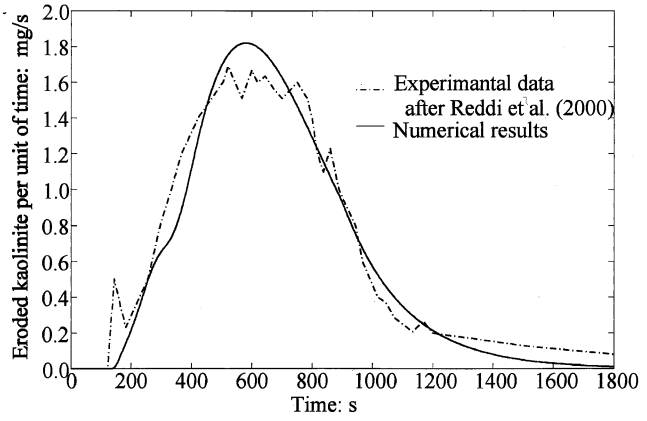

Fig. 5. Relationship between discharge rate of kaolinite and elapsed time after Reddi et al. (2000)

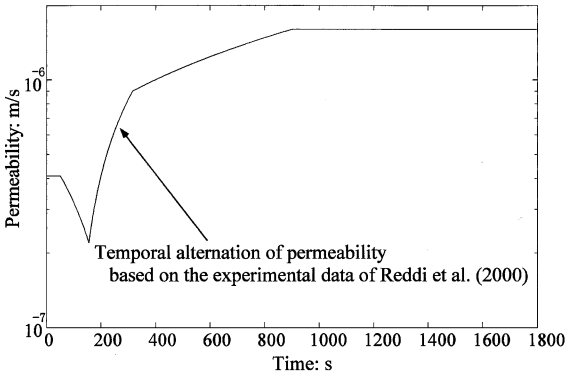

Fig. 6. Relationship between the recorded permeability and the elapsed time during the internal erosion test of Reddi et al. (2000)

$$\int_{\Omega^l} \frac{\partial nC}{\partial t} dV^l + \int_{\Omega^l} \frac{\partial v_i C}{\partial x_i} dV^l = \int_{\Omega^l} EA_e dV^l \tag{20}$$

By applying Green's formula to Eq. (20), it is reduced to

$$\int_{\Omega^l} \frac{\partial nC}{\partial t} d\Omega^l + \int_{\partial\Omega^l} Cv_i t_i^l ds^l = \int_{\Omega^l} EA_e d\Omega^l \tag{21}$$

where t_i^l is the unit normal outward vector at the boundary of the lth cell and s^l is the length of the boundary. Introducing the representative porosity and the particle concentration in the lth cell at the mth time step, $n^{l,m}$ and $C^{l,m}$, respectively, Eq. (21) is discretized into

$$V^l \frac{n^{l,m+1}C^{l,m+1} - n^{l,m}C^{l,m}}{\Delta t} + q_i^m t_{ij}^l \Delta s_j^l = V^l \frac{n^{l,m+1} - n^{l,m}}{\Delta t} \tag{22}$$

where t_{ij}^l and Δs_j^l mean the unit normal outward vector and the length of the jth boundary segment of the lth cell, as shown in Fig. 4. q_i^m in Eq. (22) denotes the flux of the eroded soil particles passing through the boundary at the mth time step. The value of the flux is given as follows, using the FVS (flux vector splitting) scheme (Toro, 1999)

$$q_i^m t_{ij}^l = C^{l,m} v_+^{l,m} + C^{r,m} v_-^{r,m} \tag{23}$$

$$v_+^{l,m} = \frac{1}{2}(v_i^{l,m} t_{ij}^l + |v_i^{l,m} t_{ij}^l|) \tag{24}$$

$$v_-^{r,m} = \frac{1}{2}(v_i^{r,m} t_{ij}^l + |v_i^{r,m} t_{ij}^l|) \tag{25}$$

Here, superscript r denotes the number of neighboring cells shearing the boundary of the lth cell, as shown in Fig. 4.

Establishing Eq. (22) and solving it for $C^{l,m+1}$ in every cell, the distribution of the particle concentration is calculated. Finally, the parameters, such as permeability, are updated and the above procedure for the calculation at one time step is repeated to the end.

REPRODUCTION OF EXPERIMENTAL RESULTS

In this section, the applicability of the numerical model presented in the previous section is verified. Reddi et al. (2000) conducted internal erosion tests using a material comprised of 70% Ottawa sand and 30% kaolinite clay by weight. A brief explanation is given here: please refer to their paper for details of their experiment.

Reddi et al. (2000) compacted the test material in a mold and prepared a cylindrical sample with the dimensions of 101.6 mm in diameter and 50 mm in thickness. The sample was saturated with and permeated by distilled water, and seepage flow in the thickness direction was generated, which caused erosion in the interior of the sample. They measured the turbidity of the effluent, which was converted to the discharge rate of kaolinite. During their experiments, they controlled the inflow rate and recorded the water pressure at the inlet of the sample.

The dashed line in Fig. 5 shows the recorded discharge rate of kaolinite. During the tests, the flow rate increased linearly from 0 to 200 ml/min up to 900 minutes and remained constant at 200 ml/min after that. Since the pore water pressure was continuously measured, an alteration of the permeability was experimentally obtained during the tests. Figure 6, which was drawn on the basis of the figure in their paper, shows the temporal alteration of the permeability during the tests.

In order to verify the proposed numerical model, a reproduction of the experimental data was carried out. The numerical results of the kaolinite discharge rate are shown as the solid line in Fig. 5. It can be seen that the

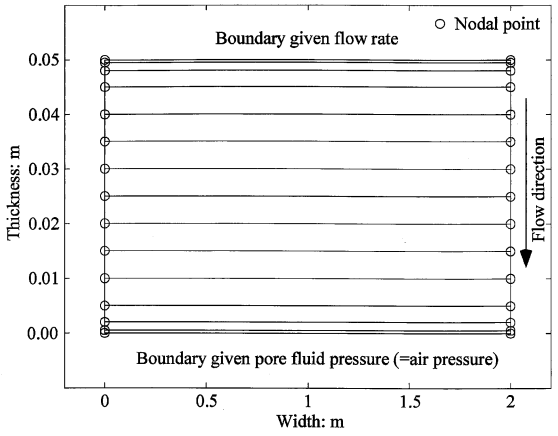

Fig. 7. Finite element mesh and boundary conditions for the test specimen

numerical results provide good agreement with the experimental data.

In this numerical analysis, the finite element mesh shown in Fig. 7 was used. The width of the mesh was arbitrarily chosen since the experiment in Reddi et al. (2000) was for a one-dimensional problem. As the boundary conditions, the flow rate equivalent to their control was imposed on the top and the atmospheric pressure was applied as the pore liquid pressure at the bottom. By integrating the kaolinite discharge rate, indicated in Fig. 5, with respect to time and obtaining the total eroded soil mass ($=1.1\times10^{-3}$ kg), the initial surface area of the erodible soil particles was determined by multiplying the value of the eroded soil weight by the specific surface area of kaolinite ($=20\times10^{3}$ m^2/kg). The surface area per unit volume A_e was obtained by dividing it by the volume of the test sample ($=4.05\times10^{-4}$ m^3). Other parameters, including the gravitational acceleration ($=9.8$ m/s^2), the density of water ($=1000$ kg/m^3), the soil particles ($=2600$ kg/m^3), and the viscosity of pure water ($=1.005\times10^{-3}$ kg/m.s) were given, and the critical shear stress ($=1.1$ Pa) and the initial porosity ($=0.27$) were provided by the results of Reddi et al. (2000). During the numerical analysis, the permeability was updated according to the changes shown in Fig. 6. Only the erodibility coefficient, α, could not be determined. Thus, its value was arbitrarily given as 5.5×10^{-8} m^3/kN·s to match the experimental data shown in Fig. 5. The erodibility coefficient for internal erosion has yet to be determined due to the great difficulty involved in doing so. Khilar et al. (1985) and Reddi et al. (2000), however, indicated that the erodibility coefficient of internal erosion is even smaller than that of surface erosion, namely, in the range of 1.0×10^{-4} to 1.0×10^{-3} m^3/kN·s. The estimated value of the coefficient, 5.5×10^{-8} m^3/kN·s, is consistent with their observations.

This analysis has shown that the numerical results seen in Fig. 5 agree well with the experimental data and that the proposed approach can reproduce the observed data sufficiently well.

EXAMPLES OF THE NUMERICAL EXPERIMENTS

The results of the previous section have indicated that the proposed approach can predict the actual internal erosion and the transport of eroded soil particles with the material parameters related to the erosion. In this section, it will also be shown that the proposed method can simulate the development of the piping phenomenon owing to the loss of soil particles, which has been difficult to analyze, after a simple erosion model is presented.

Erosion Model

The surface area of erodible soil particles per unit volume of soils, A_e, is required in order to assess how much and how fast the soils erode. In the previous section, the surface area is estimated from the experimental results of the kaolinite discharge rate. However, very few studies have been done on the erodibility within soils and it is considerably difficult to estimate the amount of erodible particles in ordinary soils with a wide range in particle distribution. Therefore, a simple model for the internal erodibility of soils is proposed here in advance of the subsequent numerical analysis.

Supposing a particle distribution curve is given, as shown in Fig. 8, the soil particles with a diameter between D_{i-1} and D_i account for the percent of P_i-P_{i-1} by weight. Letting ρ_s denote the density of the soil grains, the particles with a diameter between D_{i-1} and D_i weigh $\rho_s(1-n)(P_i-P_{i-1})$ within the unit volume of the soil, because the soil mass of the unit volume contains the soil particles of $\rho_s(1-n)$ by weight. Using the following averaged particle diameter D_i' as the representative value of the fraction

$$D_i'=\frac{D_{i-1}+D_i}{2} \tag{26}$$

the surface area of the fraction existing within the unit volume of the soil mass, A_e^i, is obtained as follows:

$$A_e^i=\rho_s(1-n)(P_i-P_{i-1})\frac{A_2(D_i')^2}{\rho_s A_3(D_i')^3} \tag{27}$$

where A_2 and A_3 are the shape coefficients used to calculate the surface area and the volume, respectively. For example, if the soil particles are spherical, the values of A_2 and A_3 are determined as π and $\pi/6$, respectively. The erodible particles are assumed to be the soil particles which are smaller than the pore size. Considering representative pore size $\hat{D}$, given by Eq. (14), with porosity n and intrinsic permeability K, the surface area of the erodible particles is determined by the following equation:

$$A_e=\sum_{D_i'<\hat{D}}A_e^i=\sum_{D_i'<\hat{D}}\frac{A_2(1-n)(P_i-P_{i-1})}{A_3D_i'} \tag{28}$$

The curve of the particle size distribution, as shown in Fig. 8, alters due to the erosion at each time step in the numerical simulation because only the particles smaller than the representative pore size $\hat{D}$ are subject to erosion. The alteration of the curve also affects the value of the representative pore size $\hat{D}$ and the surface area of erodible

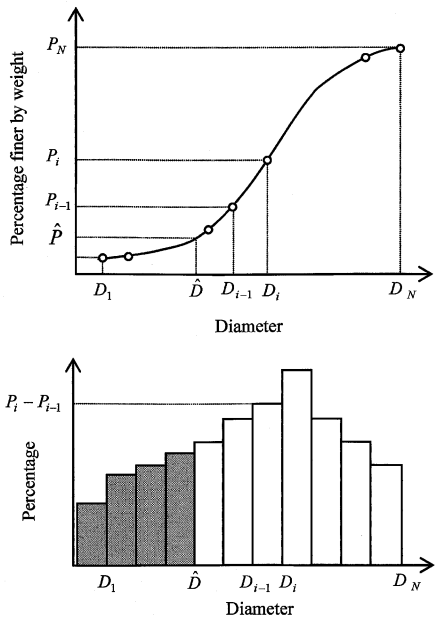

Fig. 8. Particle size distribution and representative pore size

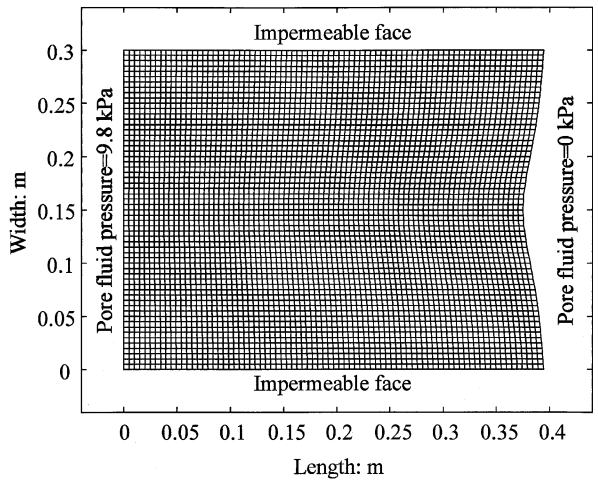

Fig. 9. Finite element mesh and boundary conditions for the horizontally-placed soil block

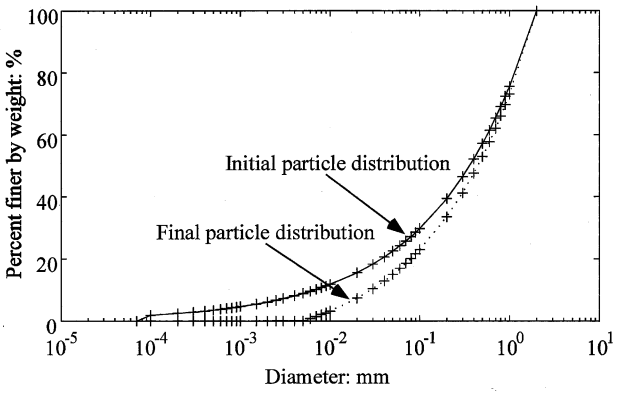

Fig. 10. Initial particle size distribution of the soil block and the final particle size after erosion

particles A_e. An explanation of how to update the particle size distribution is provided in the APPENDIX.

However, it should be noted that the above model used to determine the erodible particles and their surface area is only conceptual at present and that further investigation is required.

Due to erosion, the material parameters of the density and the viscosity of the pore liquid and the permeability vary. The density and the viscosity of the pore liquid are updated with the following equations (Julien, 1998):

$$\rho = C\rho_s + (1-C)\rho_w \tag{29}$$

$$\mu = \eta(1+2.5C) \tag{30}$$

where ρ_w and η denote the density and the viscosity of pure water, respectively. The permeability varies because of changes in the fluid viscosity, so that it is also updated as follows (e.g., Lambe and Whitman, 1979; Budhu, 2007):

$$k_s = D_r^2 \frac{\rho g}{\mu} \frac{C_T n^2}{(1-n)^3} \tag{31}$$

where C_T and D_r are the material constant and the representative particle diameter, respectively. Particle diameter D_{50}, for which 50% of the soil particles are finer by weight, is adopted as the representative particle diameter in the following numerical analysis.

Erosion within a Horizontally-placed Saturated Soil Block

As the first example of the numerical analysis with the proposed method, the internal erosion of a horizontally-placed saturated soil block is addressed here. Figure 9 shows the finite element mesh and the imposed boundary conditions. The mesh is also used as the finite volume cell. It has 4800 elements and 4941 nodal points. The soil block is 40 cm in length and 30 cm in width. As for the boundary conditions for the seepage flow of the pore liquid, pressure levels of 9.8 and 0 kPa, the atmospheric pressure, are applied to the left and the right sides, respectively, and the upper and the lower faces are assumed to be impermeable. These conditions induce the rightward flow in the figure. Referring to the experiments of Sellmeijer (2008), the right side of the soil block is slightly concave so that the seepage is concentrated in the center of the right side. In the numerical analysis, the soil block initially had porosity and permeability values of 0.36 and 1.0×10^{-6} m/s, respectively. The initial particle size distribution shown in Fig. 10 was given, whereby the soil particles were assumed to be spherical. It was supposed that the pore liquid did not initially contain the eroded particles. As for the other parameters, the gravitational acceleration of 9.8 m/s^2, the density and the viscosity of pure water of 1000 kg/m^3 and 1.002×10^{-3} kg/m.s, respectively, the density of the soil grains of 2600 kg/m^3, a critical shear stress τ_c of 0.021 Pa, and an erodibility coefficient α of 2.1×10^{-7} were assumed. The parameters of the critical shear stress τ_c and the erodibility coefficient α are the material constants and the values for clays and several soils have been experimentally investigated by ap-

plying several types of experimental apparatus (e.g., Khilar et al.,1985; Shaikh et al., 1988; Reddi et al., 2000; Indraratna et al., 2009). In this analysis, assuming that the internal erosion would be induced, the value of the critical stress τ_c(=0.021 Pa) was determined so that the erosion occurred at the center of the right side where the seepage flow velocity was relatively fast and the shear stress due to the seepage was the greatest, which is similar to the experimental procedure for observing the piping appearing at possible regions. Khilar et al. (1985) and Shaikh et al. (1988) actually reported the values of critical shear stresses close to zero and the value of 0.021 Pa in this analysis is not unrealistic. Values for the erodibility coefficient α of internal erosion, as suggested by Khilar et al. (1985) and Reddi et al. (2000), have been known to be even smaller than those of the surface erosion, namely, in the range of 1.0×10^{-4} to 1.0×10^{-3} m^3/kN·s. For this reason, a sufficiently small value of 2.1×10^{-7} m^3/kN·s was adopted. The value of the erodibility coefficient α only affects the pace with which the erosion proceeds and does not change the qualitative internal erosion process when the erosion rate is sufficiently small.

Figure 11 shows the temporal alteration of the porosity distribution within the soil block. Porosity distributions of 2000, 6000, 8000, and 20,000 minutes after the internal erosion was generated are shown in the figure. The internal erosion set out at the center of the right side where the seepage flow velocity is greater, and the eroded region (black part in Fig. 11) made leftward or backward progress and reached the left side of the soil block (2000 to 8000 minutes in Fig. 11). After that, the eroded region (black part in Fig. 11) widened a little and the erosion finally ceased. As seen in Fig. 11, the eroded region, where the porosity increased, penetrated through the soil block. The soils in the region became coarser and sparser, where the final porosity was 0.416 and the particle size distribution was changed, as shown in Fig. 10, due to the loss of fine erodible particles. The above numerical results qualitatively produce typical backward erosion which leads to piping, as observed by Sellmeijer (2008).

Internal Erosion of an Embankment

In this section, we will discuss erosion caused by a seepage flow in embankments and the effluence of fine soil particles out of them. Internal erosion develops gradually in the soil structures, which may cause them to deteriorate. Figure 12 shows the finite element mesh and the boundary conditions for the embankment. The mesh is also used for the finite volume cells; it has 10,000 elements and 10,231 nodal points. Drainage was installed at the toe of the downstream slope (the right slope in the figure). The internal erosion, initiated under the steady seepage flow and provided by the 2-meter-high impoundment, was investigated in this analysis. As the boundary conditions, values for the hydrostatic pressure were given on the upstream surface of the embankment below the impounded water level and the right extreme where the seepage water level was assumed to be the same as the ground. The base of the ground was assumed to be impermeable and seepage conditions (Neuman, 1973) were imposed on the other surface of the embankment.

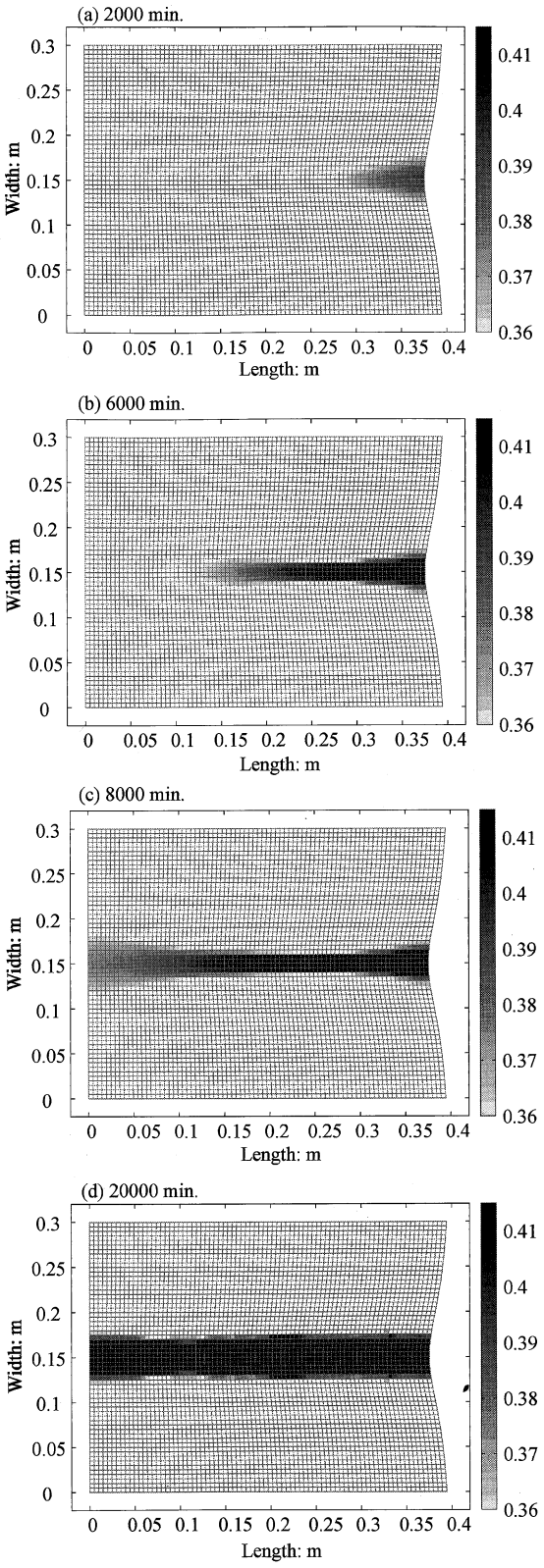

Fig. 11. Temporal change in the porosity distribution owing to erosion

The concentration of eroded soil particles within the pore liquid was initially zero throughout the embankment. Before the analysis of the internal erosion, the im-

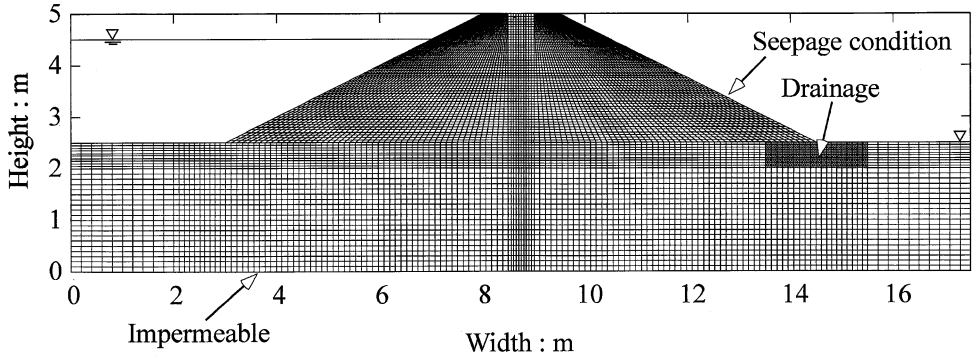

Fig. 12. Finite element mesh and boundary conditions for the embankment

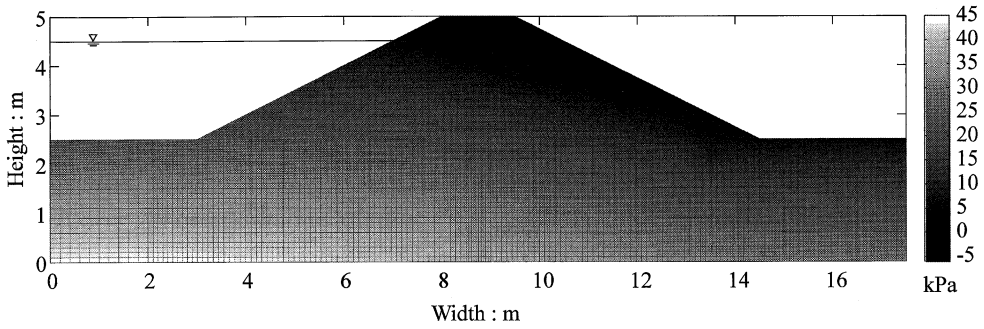

Fig. 13. Pressure distribution of pore liquid under the steady state

poundment was conducted 2 m from the bottom of the embankment by gradually increasing the water level, and then the water level was kept constant long enough to create a steady state. The calculated distribution of pore water pressure shown in Fig. 13 was adopted as the initial condition with respect to the pressure of the pore liquid without eroded soil particles. The embankment, except for the drainage, was assumed to be homogeneous and was given initial porosity and saturated hydraulic conductivity values of 0.31 and 1.0×10^{-6} m/s, respectively. The initial particle size distribution of the material used in this analysis is shown in Fig. 14 and the soil particles were assumed to be spherical. The supposed material is a sandy soil containing about 30% silts and clays, which is common in embankment construction. Material constants of $m_G=0.881$, $\alpha_G=0.297\ \mathrm{kPa}^{-1}$, and $S_{rr}=0.30$ with water retention characteristics were given, and $\alpha=0.51\times10^{-7}\ \mathrm{m^3/kN\cdot s}$ and $\tau_c=5.73\times10^{-6}$ kPa were assumed for the parameters of the erosion rate of the embankment material. The value of the critical shear stress was determined so that erosion could occur at the entrance of the drainage and the upstream slope around the impounded water level, where the seepage flow velocity is the greatest in the embankment. Therefore, the object of this numerical analysis is the development of piping, which was induced by the erosion around the most likely parts. A sufficiently small value for the erodibility coefficient was adopted as it also was for the previous analysis. Other parameters for the gravitational acceleration ($g=9.8\ \mathrm{m/s^2}$), the density of water ($\rho=1000\ \mathrm{kg/m^3}$),

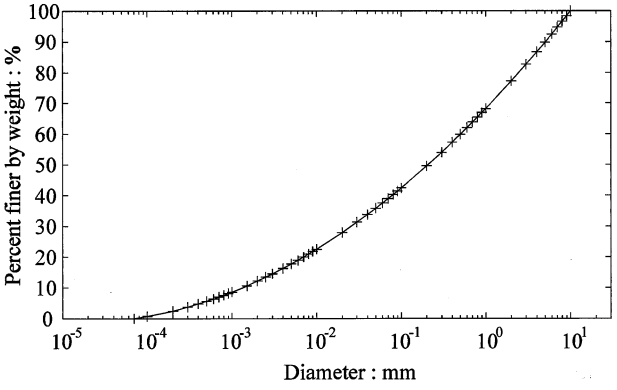

Fig. 14. Particle size distribution of the embankment material

the density of the soil particles ($\rho_s=2600\ \mathrm{kg/m^3}$), and the viscosity of the pure water ($\mu=1.002\times10^{-3}\ \mathrm{Pa\cdot s}$) were supposed. It was assumed that the drainage material was not erodible and that it had a permeability value of 1.0×10^{-3} m/s.

As time elapsed and the numerical simulation of the internal erosion within the embankment progressed, the soils upstream of the drainage and at the upstream slope close to the impounded water surface were eroded by the seepage water. In addition, the porosity there increased, because the exerted shear stress around these regions was greater than in other parts in the embankment. Figure 15 shows the porosity distribution in the embankment 2, 4, and 7 years later. The erosion around the entrance of the

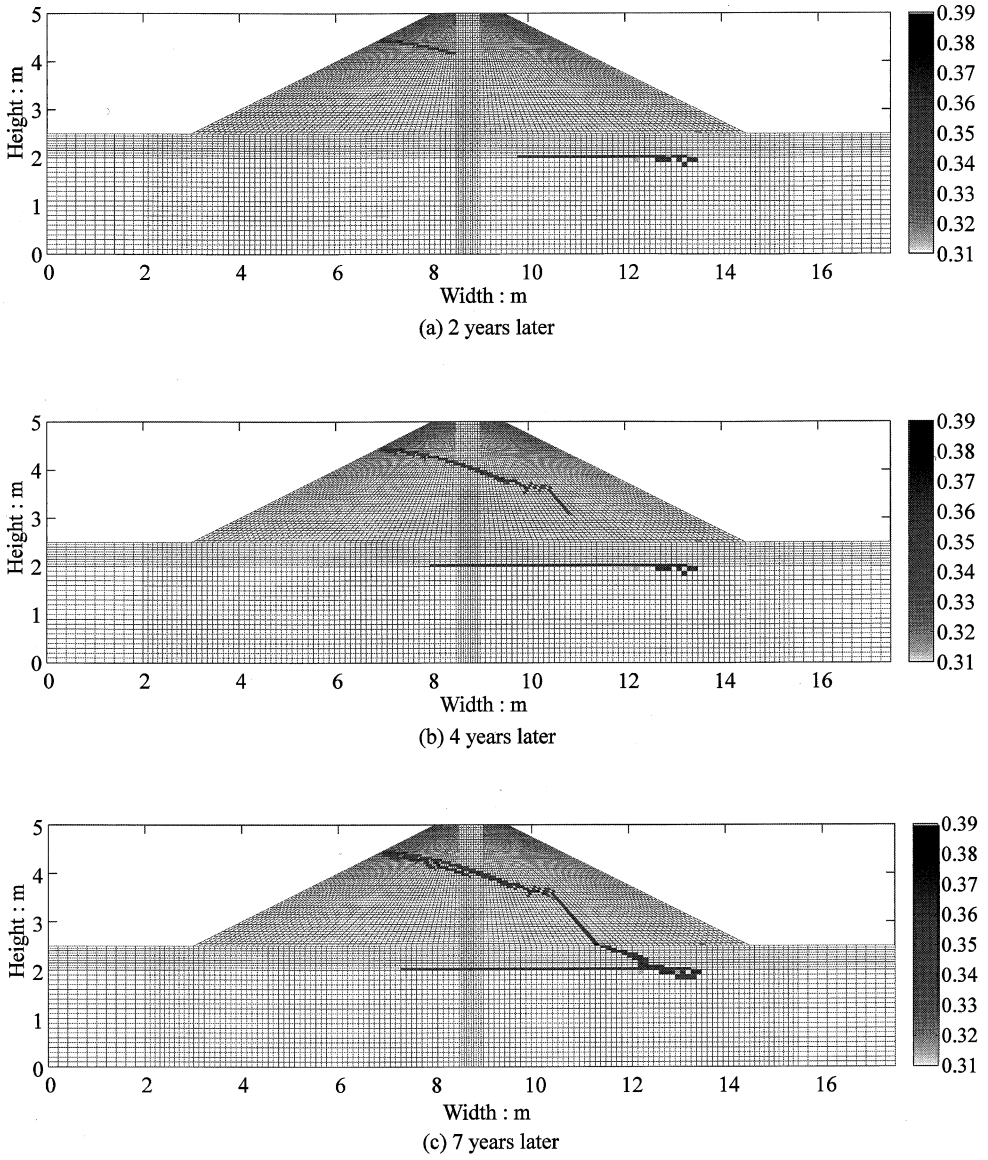

Fig. 15. Temporal alteration of the porosity distribution within the embankment

drainage developed horizontally along the bottom of the embankment, and the erosion, which started at the upstream slope, developed down the seepage surface and reached the drainage in 7 years. It is observed that the seepage flow became relatively rapid and concentrated in the coarse regions, where the porosity increased because of the erosion. A flow path clearly appeared, as shown in Fig. 15.

This numerical analysis has shown that the proposed method can qualitatively simulate local changes in the porosity of soils due to internal erosion and the seepage flow field, and that the method may be able to predict the development of piping within soil structures.

CONCLUSIONS

This paper has presented a numerical method for analyzing the internal erosion of soils leading to piping. In order to describe internal erosion, the concept of the four phases of soils has been introduced. Usage of the erosion rate of soils has enabled the Eulerian derivation of the governing equations for the seepage flow, the changes in porosity, and the transport of the detached soil particles from the soil skeleton.

By carrying out the numerical calculation, the finite element method, accurate solutions for the seepage flow field were shown to be possible, while the finite volume method allowed for easy installation and a low computational load since the method does not necessitate solving the matrices.

The proposed method reproduced the experimental results of the internal erosion tests conducted by Reddi et al. (2000), indicating that the method can predict erosion within soils if the erosion characteristics, such as the erodibility coefficient and the critical shear stress, are determined. In addition, the numerical results of the internal erosion within the horizontally-placed soil block and the embankment show that the proposed method can

describe typical backward erosion and the development of the piping path within an embankment. It is suggested that solving the initial and the boundary problems of the above governing equations allows us to extrapolate the temporal development of the piping phenomenon. The proposed method will contribute to the estimation of piping and hollows inside of soil structures when reliable erosion models within soils are established.

REFERENCES

1) Ariathurai, R. and Arulanandan, K. (1978): Erosion rates of cohesive soils, *Journal of the Hydraulic Division*, ASCE, **104**, HY2, 279–283.
2) Briaud, J. L., Ting, F. C. K., Chen, C., Cao, Y., Han, S. W. and Kwak, K. W. (2001): Erosion function apparatus for scar rate predictions, *Journal of Geotechnical and Geoenvironmental Engineering*, **127**(2), 105–113.
3) Budhu, M. (2007): *Soil Mechanics and Foundation, 2nd Edition*, John Wiley & Sons, 83.
4) Gruesbeck, C. and Collins, R. E. (1982): Entrainment and deposition of fine particles in porous media, *Soc. Petroleum Engrg. J.*, 1982(Dec.), 847–856.
5) Julien, P. Y. (1998): *Erosion and Sedimentation*, Cambridge University Press, 15.
6) Khilar, K. C., Fogler, H. S. and Gray, D. H. (1985): Model for piping-plugging in earthen structures, *Journal of Geotechnical Engineering*, ASCE, **111**(7), 833–846.
7) Lambe, T. W. and Whitman, R. V. (1979): *Soil Mechanics, SI version*, John Wiley & Sons, 283.
8) Neuman, S. P. (1973): Saturated-unsaturated seepage by finite element, *Journal of the Hydraulics Division, Proc. ASCE*, **99**, HY12, 2233–2250.
9) Foster, M., Fell, R. and Spannagle, M. (2000a): The statistics of embankment dam failures and accidents, *Can. Geotech. J.*, **37**, 1000–1024.
10) Foster, M., Fell, R. and Spannagle, M. (2000b): A method for assessing the relative likelihood of failure of embankment dams by piping, *Can. Geotech. J.*, **37**, 1025–1061.
11) Fujisawa, K., Murakami, A. and Nishimura, S. (2009): Numerical analysis of piping development induced by loss of soil particles, *Journal of Applied Mechanics*, JSCE, **12**, 395–403 (in Japanese).
12) Indraratna, B., Muttuvel, T. and Khabbaz, H. (2009): Modelling the erosion rate of chemically stabilized soil incorporating tensile force-deformation characteristics, *Can. Geotech. J.*, **46**, 57–68.
13) Izumi, N. and Parker, G. (2000): Linear stability analysis of channel inception: downstream-driven theory. *Journal of Fluid Mechanics*, **419**, May, 239–262.
14) Meyer, W., Schuster, R. L. and Sabol, M. A. (1994): Potential for seepage erosion of landslide dam, *Journal of Geotechnical Engineering*, **120**(7), 1211–1229.
15) Ojha, C. S. P., Sigh, V. P. and Adrian, D. D. (2003): Determination of critical head in soil piping, *Journal of Hydraulic Engineering*, **129**(7), 511–518.
16) Reddi, L. N. and Bonala, M. V. S. (1997): Analytical solution for fine particle accumulation in soil filters, *Journal of Geotechnical and Geoenvironmental Engineering*, **123**(12), 1143–1152.
17) Reddi, L. N., Lee, In-M and Bonala, M. V. S. (2000): Comparison of internal and surface erosion using flow pump test on a sand-kaolinite mixture, *Geotechnical Testing Journal*, **23**(1), 116–122.
18) Richards, K. S. and Reddy, K. R. (2007): Critical appraisal of piping phenomenon in earth dams, *Bull. Eng. Geol. Environ.*, **66**, 381–402.
19) Robinson, K. M. and Hanson, G. J. (1994): A deterministic head-cut advance model, *Transactions of the ASAE*, **37**(5), 1437–1443.
20) Sellmeijer, H. (2008): *Mechanism of Piping*, Document for Delft Geoacademy Course of Understanding Dike Safety, Deltares.
21) Shaikh, A., Ruff, J. F. and Abt, S. R. (1988): Erosion rate of compacted Na-montmorillonite soils, *Journal of Geotechnical Engineering*, **114**(3), 296–305.
22) Skempton, A. W. and Brogan, J. M. (1994): Experiments on piping in sandy gravels, *Geotechnique*, **44**(3), 449–460.
23) Toro, E. F. (1999): *Riemann Solvers and Numerical Method for Fluid Dynamics, 2nd edition*, Springer.
24) van Genuchten, M. Th. (1980): A closed-form equation for predicting the hydraulic conductivity of unsaturated soils, *Soil. Sci. Soc. Am. J.*, **44**, 892–898.
25) Wan, C. F. and Fell, R. (2004): Investigation of rate of erosion of soils in embankment dams, *Journal of Geotechnical and Geoenvironmental Engineering*, **130**(4), 373–380.

APPENDIX

Suppose that we have a curve of the particle size distribution, as shown in Fig. 8, at mth time step and that the volume of the soil skeleton $\Delta V_{ss}(=V_{ss}^{m+1}-V_{ss}^{m}<0)$ within a soil mass is subjected to erosion during the time interval of Δt between mth and $m+1$th time step. In this APPENDIX, the same notations as in the main body of this paper are adopted and the superscript similarly denotes the time step. The erodible soils are composed of particles smaller than the representative pore size of the soil mass $\hat{D}^m$, so that the soils eroded during the time interval include the following fractions in weight f_i^m of the soil particles between D_{i-1} and D_i in diameter:

$$f_i^m=\begin{cases}\dfrac{P_i^m-P_{i-1}^m}{\hat{P}^m}, & D_i\le\hat{D}^m\\ \dfrac{\hat{P}^m-P_{i-1}^m}{\hat{P}^m}, & D_{i-1}<\hat{D}^m<D_i\\ 0, & D_{i-1}\ge\hat{D}^m\end{cases} \tag{A1}$$

Equation (A1) means that the eroded soils have the same proportion of the particle sizes as the current distribution of the fine particles within the soil skeleton. Considering that the volume $\Delta V_{ss}(<0)$ is lost from the soil skeleton owing to the erosion, its weight reduces by $\Delta V_{ss}/\rho_s$ and the weight of the soil particles between D_{i-1} and D_i in diameter, included in the soil skeleton, decreases by $f_i^m\cdot\Delta V_{ss}/\rho_s$ into the following value w_i^{m+1} at $m+1$th time step:

$$w_i^{m+1}=\frac{V_{ss}^m}{\rho_s}\cdot\frac{P_i^m-P_{i-1}^m}{100}+\frac{\Delta V_{ss}}{\rho_s}\cdot f_i^m \tag{A2}$$

Therefore, the percentage p_i^{m+1} of the partial weight w_i^{m+1} to the weight of all soil particles composing the skeleton at $m+1$th time step can be determined as follows:

$$\begin{aligned}p_i^{m+1}&=\frac{\rho_s w_i^{m+1}}{V_{ss}^m+\Delta V_{ss}}\times 100\\&=\frac{V_{ss}^m}{V_{ss}^{m+1}}(P_i^m-P_{i-1}^m)+\frac{\Delta V_{ss}}{V_{ss}^{m+1}}\cdot f_i^m\times 100\end{aligned} \tag{A3}$$

Using the following relationship

$$\frac{V_{ss}^m}{V_{ss}^{m+1}}=\frac{1-n^m}{1-n^{m+1}},\quad \frac{\Delta V_{ss}}{V_{ss}^{m+1}}=-\frac{n^{m+1}-n^m}{1-n^{m+1}}, \tag{A4}$$

Eq. (A3) is rewritten into

$$p_i^{m+1}=\frac{1-n^m}{1-n^{m+1}}(P_i^m-P_{i-1}^m)-\frac{n^{m+1}-n^m}{1-n^{m+1}}\cdot f_i^m\times 100 \quad \text{(A5)}$$

In the numerical analysis, the governing Eqs. (8), (9) and (11) are solved and the spatial distribution of the porosity can be obtained at each time step. Hence, Eq. (A5) can update the particle size distribution with the calculated value of the porosity after the simulation from mth to $m+1$th time step. To obtain the grain size accumulation curve, the percentage in weight P_i^{m+1} of the soil particles finer than D_i in diameter is calculated by $P_i^{m+1}=\sum_{j\le i} p_j^{m+1}$.